REPORT DOCUMENTATION PAGE

Form Approved
OMB No. 0704-0188

PLEASE DO NOT RETURN YOUR FORM TO THE ABOVE ORGANIZATION.

1. REPORT DATE *(DD-MM-YYYY)*	2. REPORT TYPE	3. DATES COVERED *(From - To)*
06-06-2008	Journal Article	

4. TITLE AND SUBTITLE
Optimizing Performance of a Microwave Salinity Mapper: STARRS L-band Radiometer Enhancements

5a. CONTRACT NUMBER

5b. GRANT NUMBER

5c. PROGRAM ELEMENT NUMBER
0602435N

6. AUTHOR(S)
Derek M. Burrage, Joel C. Wesson, M.A. Goodberlet, Jerry Miller

5d. PROJECT NUMBER

5e. TASK NUMBER

5f. WORK UNIT NUMBER
73-6629-05-5

7. PERFORMING ORGANIZATION NAME(S) AND ADDRESS(ES)
Naval Research Laboratory
Oceanography Division
Stennis Space Center, MS 39529-5004

8. PERFORMING ORGANIZATION REPORT NUMBER
NRL/JA/7330-05-5315

9. SPONSORING/MONITORING AGENCY NAME(S) AND ADDRESS(ES)
Office of Naval Research
800 N. Quincy St.
Arlington, VA 22217-5660

10. SPONSOR/MONITOR'S ACRONYM(S)
ONR

11. SPONSOR/MONITOR'S REPORT NUMBER(S)

12. DISTRIBUTION/AVAILABILITY STATEMENT
Approved for public release, distribution is unlimited.

13. SUPPLEMENTARY NOTES

14. ABSTRACT
Airborne microwave radiometers for salinity remote sensing have advanced to a point where operational surveys can be conducted over the inner continental shelf to observe the evolution of freshwater plumes emanating from rivers and estuaries. To determine seawater microwave emissivity, and hence conductivity and salinity, precisely and accurately demands high instrument sensitivity, stability, and sampling rates; such requirements involve significant design trade-offs. The Salinity, Temperature, and Roughness Remote Scanner (STARRS) was developed to enhance these features relative to existing instruments. The authors describe here key elements of the STARRS design and the results of early performance assessments and deployments. During early deployments, the instrument performed well in areas of moderate to high salinity signal-to-noise ratio, but more homogenous areas revealed band-limited random signal fluctuations on the order of a 6-min period and 1-K amplitude that were of ...

15. SUBJECT TERMS
STARRS, salinity, Airborne microwave radiometers

16. SECURITY CLASSIFICATION OF:			17. LIMITATION OF ABSTRACT	18. NUMBER OF PAGES	19a. NAME OF RESPONSIBLE PERSON
a. REPORT	b. ABSTRACT	c. THIS PAGE			Derek Burrage
Unclassified	Unclassified	Unclassified	UL	18	19b. TELEPHONE NUMBER *(Include area code)* 228-688-5241

Optimizing Performance of a Microwave Salinity Mapper: STARRS L-Band Radiometer Enhancements*

DEREK M. BURRAGE AND JOEL C. WESSON

Naval Research Laboratory, Stennis Space Center, Mississippi

MARK A. GOODBERLET

ProSensing Inc., Amherst, Massachusetts

JERRY L. MILLER

Consortium for Oceanographic Research and Education, Washington, D.C.

(Manuscript received 18 November 2005, in final form 4 May 2007)

ABSTRACT

Airborne microwave radiometers for salinity remote sensing have advanced to a point where operational surveys can be conducted over the inner continental shelf to observe the evolution of freshwater plumes emanating from rivers and estuaries. To determine seawater microwave emissivity, and hence conductivity and salinity, precisely and accurately demands high instrument sensitivity, stability, and sampling rates; such requirements involve significant design trade-offs. The Salinity, Temperature, and Roughness Remote Scanner (STARRS) was developed to enhance these features relative to existing instruments. The authors describe here key elements of the STARRS design and the results of early performance assessments and deployments. During early deployments, the instrument performed well in areas of moderate to high salinity signal-to-noise ratio, but more homogenous areas revealed band-limited random signal fluctuations on the order of a 6-min period and ~1-K amplitude that were of internal origin. Detailed analyses of laboratory and field tests revealed that internal "flicker," or $1/f$ noise (having spectral roll-off proportional to the reciprocal of frequency f), was the main source of these fluctuations. The instrument was modified to eliminate the random fluctuations and to further enhance sensitivity and stability. Laboratory tests and recent field deployments show that the upgrade improved instrument performance dramatically, to the extent that continental shelf scale areas with relatively homogenous salinity distributions can now be surveyed reliably using STARRS.

1. Introduction

Technology for passive microwave remote sensing of sea surface salinity (SSS) has progressively advanced in the last two decades, so that operational airborne mapping of coastal salinity distributions at ~0.5-km spatial scales is now possible (see Burrage et al. 2003, 2002a for brief reviews), and satellite missions intended to map open ocean SSS and terrestrial soil moisture globally with a spatial resolution of order 50 km are under development (Lagerloef et al. 1995). These missions include the European Space Agency (ESA) Soil Moisture and Ocean Salinity (SMOS) mission (Kerr et al. 2001) and the National Aeronautics and Space Administration (NASA) *Aquarius* mission (Le Vine et al. 2006).

In the early 1990s, the Microwave Remote Sensing Laboratory (MIRSL) at the University of Massachusetts at Amherst, along with Quadrant Engineering Inc. (now ProSensing Inc.) and funding from the National Oceanic and Atmospheric Administration (NOAA), developed a single-channel, multibeam L-band microwave imaging instrument called the Scanning Low Frequency Microwave Radiometer (SLFMR; Goodberlet and Swift 1993). The SLFMR was subsequently dupli-

* Naval Research Laboratory Contribution Number NRL/JA/7330-05-5313.

Corresponding author address: Dr. Derek M. Burrage, Ocean Sciences Branch, Code 7332, Naval Research Laboratory, Stennis Space Center, MS 39529.
E-mail: burrage@nrlssc.navy.mil

DOI: 10.1175/2007JTECHO461.1

TABLE 1. Original STARRS L-band radiometer performance specifications design (column 3) delivered (column 4). Adapted from ProSensing Inc. (2001, their Table 4.1, p. 13).

Component assembly	Parameter	Design specification	Delivered specification
Receivers	Type	Hach	Yes
	Frequency	1.413 GHz	Yes
	Bandwidth	24 MHz	Yes
	1-s NEDT	0.16 K	0.34 K* 0.38 ± 0.08 K
	Range	3–300 K	0–999 K
Antenna	Type	8 × 8 microstrip patch array	Yes
	Polarization	Linear, Vertical	Linear, Vertical
	Beamwidth (3 dB) Along/cross track	15°/17°	15°/12°–16.5°
	Beam incidence angles (3 L–3 R)	−37°, −22°, −8°, 8°, 22°, 37°	−38.5°, −21.0°, −6.5°, 7.5°, 22.0°, 38.5°
	Max sidelobe (dB) below main lobe level (3 L–3 R) Along/cross track	20/12	24/(12, 11, 12, 14, 13, 11)
System	Size (L × W × H)	1.016 × 1.016 × 0.178 m	1.016 × 1.016 × 0.254 m
	Weight	120 lb or 54.4 kg	145 lb or 65.8 kg
	Electronics power needs	80 W	73 W
	Max heater power needs	800 W	600 W @ 50 V

* NEDT standardized to 1 s, estimated using procedures described in ProSensing Inc. (2001, p. 13; upper value) (2002; lower value) as discussed in text.

cated for an Australian research consortium. These instruments, designed to map SSS from an aircraft, were used in a variety of remote sensing surveys of estuarine and coastal regions (Goodberlet et al. 1997; Miller et al. 1998; Miller 2000; D'Sa et al. 2001; Johnson et al. 2002, unpublished manuscript; Burrage et al. 2002b,c, 2003). Based on this experience and a desire to improve instrument sensitivity and calibration, specifications were developed (Table 1) for a new six-channel microwave instrument system, the Salinity, Temperature and Roughness Remote Scanner (STARRS; ProSensing Inc. 2001; Miller and Goodberlet 2004). Design and development of STARRS by Quadrant Engineering began under Naval Research Laboratory (NRL) contract in May 2000 and it was first deployed operationally in October 2001. Unlike its predecessor, STARRS combines three radiometers in one system. These operate in the L, C, and IR bands to measure surface conductivity, sea surface roughness, and sea surface temperature (SST), respectively. Although salinity retrieval requires data on all three surface properties, here we focus primarily on the performance of the L-band radiometer.

After 4 yr of progressive development and deployments in a variety of estuarine and coastal ocean settings, it is timely to reexamine the original STARRS design (Fig. 1), discuss subsequent performance enhancements, and demonstrate its current capabilities. This is the primary goal of the paper. Increasingly, microwave radiometer design features and functions that were previously implemented in hardware (such as antenna/reference load 'chopping ') are now executed in software, while data processing is carried out in real time or, optionally, in a postprocessing mode. The resulting operational flexibility allows the instrument to be modified 'on the fly, " that is, without changing hardware. Software modifications usually at least include changes to uniform or even irregular sampling times and intervals, but they may extend to synthetic beam forming, as in the electronically steered thinned array radiometer (ESTAR) (Le Vine et al. 1994) and other traditional hardware functions. Thus, sampling schemes can be optimized for particular applications. STARRS was designed from the outset to allow such sampling flexibility; for example, sensitivity could be enhanced by increasing the time spent observing the antenna versus the thermally stabilized internal loads.

Though advantageous, the resulting sampling complexity can make objective performance intercomparisons among instruments with different hardware characteristics difficult. This can be partly addressed by devising analysis techniques that account for complex sampling sequences and that reduce the resulting performance measures to standard time intervals; for example, standardizing Noise Equivalent Delta Temperature (NEDT) measurements to a 1-s interval (Goodberlet and Mead 2006). Complications arise if the noise spectrum of a particular instrument is not 'white, " in which case the NEDT is an incomplete or misleading measure of relative performance. In this case, as we

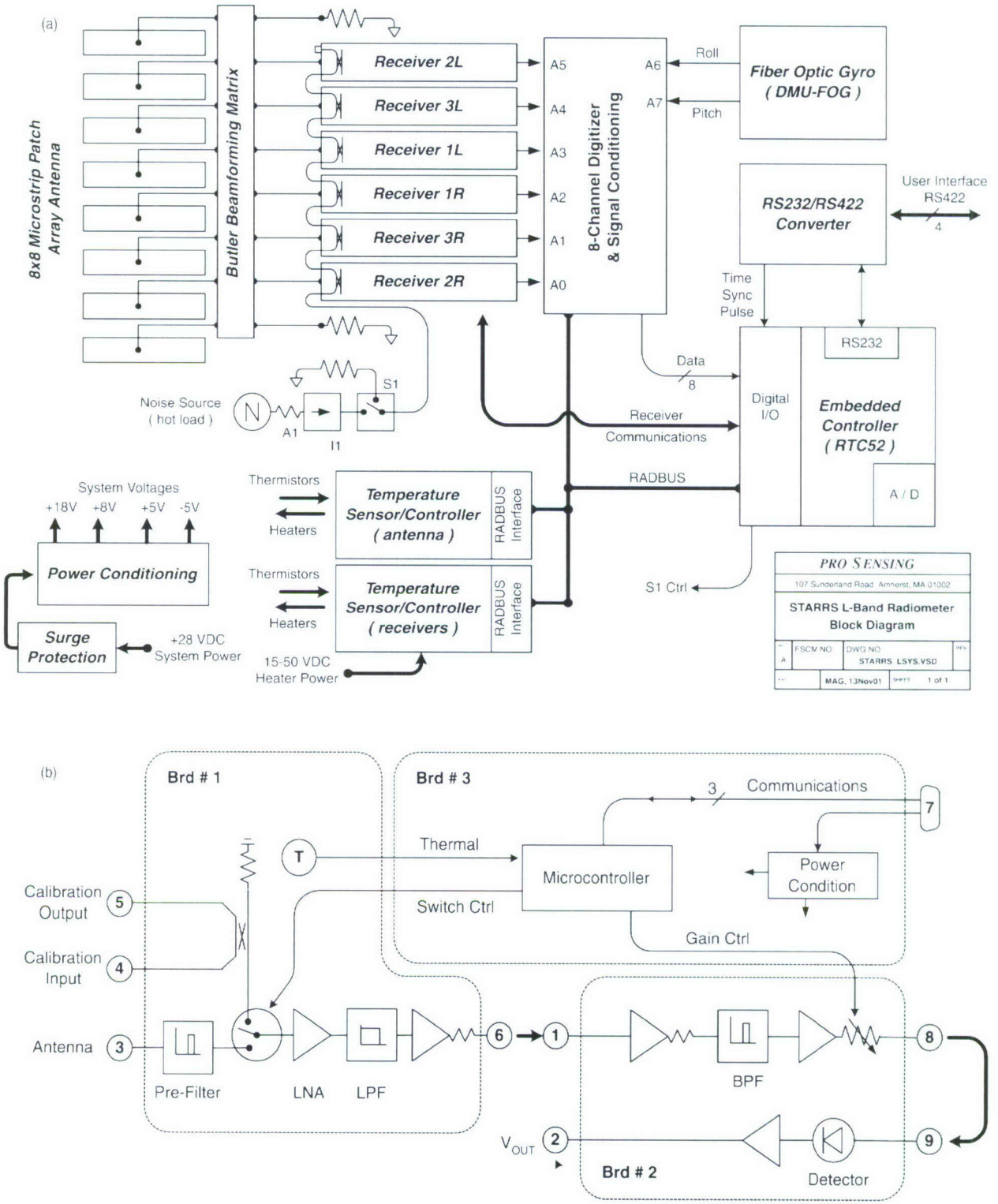

FIG. 1. STARRS schematics of (a) L-band assembly comprising multibeam antenna and receiver system and (b) L-band receiver design.

found while evaluating the original STARRS design, more general (e.g., spectral) performance measures are needed.

We first describe STARRS design improvements relative to the SLFMR. We then evaluate STARRS initial performance in laboratory and field tests with respect to instrument calibration, sensitivity, and stability. This analysis revealed the presence of $1/f$ noise. This type of noise is not readily detected using traditional performance criteria such as NEDT, which tend to emphasize short time scales. We then describe hardware and software modifications made to reduce the noise and evaluate the enhanced system using further laboratory and field tests, and we also discuss more advanced performance measures. Optimization of the sampling control software is then considered. Finally, possible refinements to extend the range of applications and functionality of STARRS are discussed. The paper concludes with a summary of the main design enhancements of STARRS and the intended future developments and applications.

2. Design considerations

Both the SLFMR and STARRS have eight-beam, vertically polarized L-band radiometers with a 64-element (8×8) antenna array and an 8-port Butler matrix beam former operating at 1.4 GHz with 24 MHz amplifier bandwidth (Fig. 1a; Table 1). The antenna array, which operates interferometrically, is phased to synthesize a single main beam antenna lobe in the along-track direction and eight main lobes across track. The beams have nominal half-power widths of 17° and 15° along and across track, respectively, and point downward and to either side of the aircraft at incidence angles of ±7°, 22°, 37°, and 65° from nadir. Signals from the six inner beams have sidelobes with power at least 11 dB down in the across-track direction and at least 20 dB down in the along-track direction. The antenna efficiency is better than 90% within a sector smaller than 1.25 times the half-power beamwidth (~20°). Given that salinity differences between the main beam and sidelobe fields of view are usually small (less than ~5 psu, even in frontal areas), antenna performance is quite adequate for salinity mapping purposes. The six inner beams are, hereafter, labeled sequentially left to right: 3L, 2L, 1L, 1R, 2R, and 3R. The outer two 65° beams, 4L and 4R, exhibit poor sidelobe performance and are not used.

In both instruments, the L-band radiometer electronic components are housed in a thermally insulated and regulated stainless steel enclosure, the lower surface of which forms a ground plane supporting the antenna elements inside a fiberglass radome. Integrated controllers sense temperature by using thermistors distributed around the enclosure and the radome. These regulate internal heaters to keep air temperatures inside the enclosure constant within a few degrees of an above-ambient set point temperature (typically 40° and 35°C for the SLFMR and STARRS, respectively). The sensors also monitor the physical temperatures of critical components such as the receiver amplifiers, Butler matrix, and hot and cold reference loads. Once warmed up, the individual component temperatures remain steady to within less than 1°C, but mean temperatures of specific components may differ because of differential self-heating and internal temperature gradients. Temperature gradients are usually more pronounced inside the radome, which shields the thermally regulated enclosure from the airstream. The various internal temperatures are employed as independent variables in the multiple regression procedure used to estimate the L-band radiometer calibration coefficients. In this way, the effects of internal temperature variations on instrument response are compensated for during processing, thus ensuring a thermally stable response.

The SLFMR possesses a single microwave receiver functioning as a pulsed noise injection Dicke radiometer (Dicke 1946; Ulaby et al. 1981; Skou 1989). This polls the eight beams sequentially in the across-track direction. Burrage et al. 2002a give a more detailed description of the instrument design and present a functional simulation in MATLAB/SIMULINK (The Mathworks Inc.). Its "balanced" negative feedback design, implemented in hardware, effectively cancels internal receiver noise and amplifier gain variations at the expense of a factor-of-2 reduction in sensitivity in comparison with an ideal total power radiometer [Ulaby et al. 1981, their Table 6.4 and Eq. (6.83)].

SLFMR performance has been evaluated both in the laboratory and during field surveys conducted in the United States and Australia (Miller et al. 1998; Miller 2000; D'Sa et al. 2001; Goodberlet et al. 1997; Burrage et al. 2002a,c, 2003; Prytz et al. 2002). For the Australian SLFMR, Burrage et al. (2002b) estimated the effective radiometric sensitivity, or single-sample NEDT (at 0.5-s sample intervals), at 0.5 K with a daily calibration drift of ±1.5 K, based on the manufacturer's calibration formula. This corresponded to an estimated salinity precision and an accuracy of 1 and 3 psu, respectively. Field data exhibited significant variations in mean brightness temperature levels on adjacent beams caused by beam calibration errors. These errors manifested as fluctuations in the overall salinity levels and as stripes in the resulting maps. Prytz et al. (2002) reduced them by including the Butler matrix physical tempera-

ture among the calibration independent-variables and by calibrating over the full range of internal instrument variations, including the instrument warm-up phase. Analyzing field data from the U.S. SLFMR, Burrage et al. (2002c) found that significant variations in beam calibration offset between missions (typically 1–3 K). Both the U.S. and Australian studies (Burrage et al. 2002c; Prytz et al. 2002) concluded that laboratory and sky calibrations were needed before and after each mission to account for calibration drift. Despite its modest sensitivity and drift susceptibility, the SLFMR produced useful oceanographic information in settings with a wide dynamic range in salinity (Burrage et al. 2002c). Its performance thus provided a useful benchmark for evaluating STARRS.

In contrast to the SLFMR, the STARRS L-band radiometer is a true multichannel instrument with six receivers, each dedicated to measuring microwave brightness temperature T_b from one of the six inner beams (Fig. 1b). Assuming uncorrelated beam signals, this design change alone yields a theoretical $1/\sqrt{6}$ improvement in instrument sensitivity, because the signals from each of the beams can be observed simultaneously, obviating the need for polling. To further optimize the noise performance, Hach (1968) instrument principles were implemented in STARRS. This contrasts with the Dicke design used in the SLFMR (Burrage et al. 2002a). Because the Hach design can be partially implemented in software, averaging times for observing the antenna and reference load brightness temperature signals can be varied to optimize the sensitivity. A key assumption made in the original STARRS design setup is that the reference loads (noise sources) are sufficiently stable, such that the observing (sampling and averaging) time of the antenna signal can be increased in relation to that of the reference noise signals, which improves the NEDT. As we shall see later, this assumption is not generally valid, due more to the deleterious effects of receiver noise and gain variations than to drift in reference noise temperatures or inaccuracies in the measurement of the physical temperatures.

Unlike the SLFMR and classic Hach designs that use hardware feedback loops to cancel receiver noise and amplifier gain variations, STARRS performs this function in software (a term which, henceforth, may include programmable firmware or embedded software). This greatly enhances sampling flexibility, allowing the noise performance to be optimized. As we show later, a drawback of this approach not found in analog systems like the SLFMR is that the chopping rate is limited by the analog-to-digital (AD) conversion rate, which must be enhanced to realize optimal performance.

3. Preliminary performance assessment

STARRS was first flown operationally in the northern Gulf of Mexico, as part of the NRL Coastal Buoyancy Jet (CoJet) experiment, CoJet-IV, conducted 7–14 October 2001, with passes over an oceanographic research vessel and instrumented buoy. The L-band radiometer appeared to perform satisfactorily. However, unexpectedly large signal variations hindered attempts at field calibration, and at that stage it was not obvious whether these fluctuations were environmental or internal to the aircraft and/or instrument. Scheduling pressures did not allow this issue to be addressed before the instrument was shipped to Europe to be flown on a different type of aircraft, as a key component of the European Space Agency's EuroSTARRS experiment. The experiment deployed STARRS to generate airborne remote sensing data for testing soil moisture and SSS retrieval algorithms, in preparation for ESA's SMOS satellite mission. Unfortunately, STARRS signal variations remained high, even over areas that in situ ship and buoy data showed were relatively homogenous, indicating that sensitivity was compromised by noise. The noise problem, independently identified by our European colleagues, became obvious during subsequent field data analysis (Wesson et al. 2003). A crucial aspect of this analysis, confirmed by laboratory tests, was that the noise could not be removed without excessive averaging, which compromised spatial resolution. The remainder of this section describes the performance and noise characteristics of the instrument at that point in its development. The subsequent section shows how the issue was resolved. (The reader wishing to skip the details of the instrument's preupgrade performance in an initial reading can proceed directly to section 4.)

a. Performance assessment in laboratory

1) INSTRUMENT CALIBRATION

The calibration procedure (ProSensing Inc. 2001) is effectively a two-point calibration with ambient (laboratory) and cold (sky) reference brightness temperatures, T_{ref}, compared to observed target brightness temperatures, T_b, measured by each beam over a range of internal component temperatures. Internal temperatures include the warm and hot load physical temperatures (proportional to their brightness temperatures to a good approximation) and the antenna feed temperature, computed as the mean temperature from four thermistors distributed around the radome. The internal temperatures are used as independent variables in the calibration regression equation of T_{ref} versus T_b, together with the output voltage ratio

TABLE 2. STARRS pre- and postupgrade sampling schemes. (columns 1-3) Number of samples and sampling intervals (cell upper), total sample times (dwell in the postupgrade case) plus load switching overhead (middle), and those times expressed as a percentage of the cycle time. (column 4) Chopping period (gamma calculation; upper), nominal sampling cycle time (middle), and the total sampling time and overhead, expressed as a percentage of the cycle time.

Scheme	Warm load	Hot + warm load	Antenna feed	Chop period cycle time percent 100%
		Preupgrade		
Repeats per cycle	2	2	4	
Sampling	3 @ 0.46 s	3 @ 0.46 s	30 @ 0.46 s	0.46 s
Interval + overhead	1.4 + 5.8 s	1.4 + 5.8 s	13.8 + 0.46 s	85.84 s
Cycle percent	3.3% + 13.5%	3.3% + 13.5%	64.3% + 2.1%	64.3% + 33.6%
		Postupgrade		
Repeats per cycle	1	1	1	
Sampling	64 @ 0.0125 s	32 @ 0.0125 s	32 @ 0.0125 s	1.96 s
Interval + overhead	0.8 + 0.1s	0.4 + 0.1 s	0.4 + 0.16 s	1.96 s
Cycle percent	40.8% + 5.1%	20.4% + 5.1%	20.4% + 8.2%	81.6% + 18.4%

$$\gamma = (Vw - Va)/(Vh - Vw), \quad (1)$$

where Va, Vw, and Vh are output voltages when the receiver views the antenna, internal warm load, and hot load, respectively. The calibration equation is

$$T_a = a_0 + a_1 T_w + a_2 \gamma + a_3 \gamma T_H + a_4 T_{\mathrm{FE}}, \quad (2)$$

where a_0, a_1, a_2, a_3, and a_4 are calibration coefficients, T_a is the antenna brightness temperature, T_w and T_H are the physical temperatures of the warm and hot load, respectively (assumed to be linearly related to their brightness temperatures), T_{FE} is the antenna feed temperature, and γ is defined in Eq. (1).

Theoretically, all receiver noise and gain variations cancel out in γ. However, because the samples are sequential and of finite duration, these are effectively eliminated only if the chopping period between antenna and loads is shorter than the time scale of those variations. STARRS was calibrated on 21 September 2001 and 26 January 2002; dates spanning the Euro-STARRS deployments of 17-23 November 2001. Typical rms regression residuals of ~0.8 K were obtained. Calibration offsets changed by 2.5 to 11.8 K, depending on beam, over the intervening 4-month period, while γ calibration slopes a_2 and a_3 changed less than 2.6%. Beam-averaged drift was thus 1.6 K month^{-1}. Euro-STARRS investigators were provided with a time-weighted linear interpolation of the two calibration coefficient vectors.

2) INSTRUMENT SENSITIVITY

The original estimates of system NEDT for STARRS (Table 1) were based on standard deviations of 10 randomly selected 60-s laboratory datasets, sampled at 0.46-s intervals (Table 2) during an experiment performed at ProSensing Inc. on 21 September 2001 (ProSensing Inc. 2001, their Table 4.1, p. 13), and on the 1-s Allan deviation from tests of about 20 min, sampled at 1-s intervals and conducted at ProSensing in July 2002 (ProSensing Inc. 2002). The NEDT values obtained were 0.34 and 0.38 ± 0.08 K, respectively. The former value has been standardized to 1-s intervals to match the latter by assuming a white noise process. The latter showed significant scatter among the beams. This probably arose, as later investigations revealed, from variable low noise amplifier (LNA) performance and residual flicker noise, which was evident despite the tendency of first differencing inherent in the Allan deviations to remove short-term trends. The 60-s records were probably too short to reveal these effects, and both sets of results could be regarded as optimistic, given the shortness of the tests.

3) INSTRUMENT STABILITY

When observed brightness temperature time series from the laboratory and sky calibration conducted on 26 January 2002 were examined, a quasi-periodic variation with a period of approximately 6 min appeared in both datasets. Once this characteristic process was identified, we determined whether its source was external (i.e., generated in the laboratory or field environment) or internal (i.e., generated by components or component interactions within the instrument). Observed T_b time series from each STARRS radiometer beam in a 3-h laboratory test conducted on 1 May 2002 are shown in Fig. 2a (discussion of Fig. 2b and corresponding panels of Figs. 3b, 4b is deferred until a later section). This test was performed in the laboratory, with the instrument surrounded by microwave-absorbing material and a grounded wire net (Faraday cage) isolating it from external electromagnetic fields. This clearly showed that the source of the noise problem was

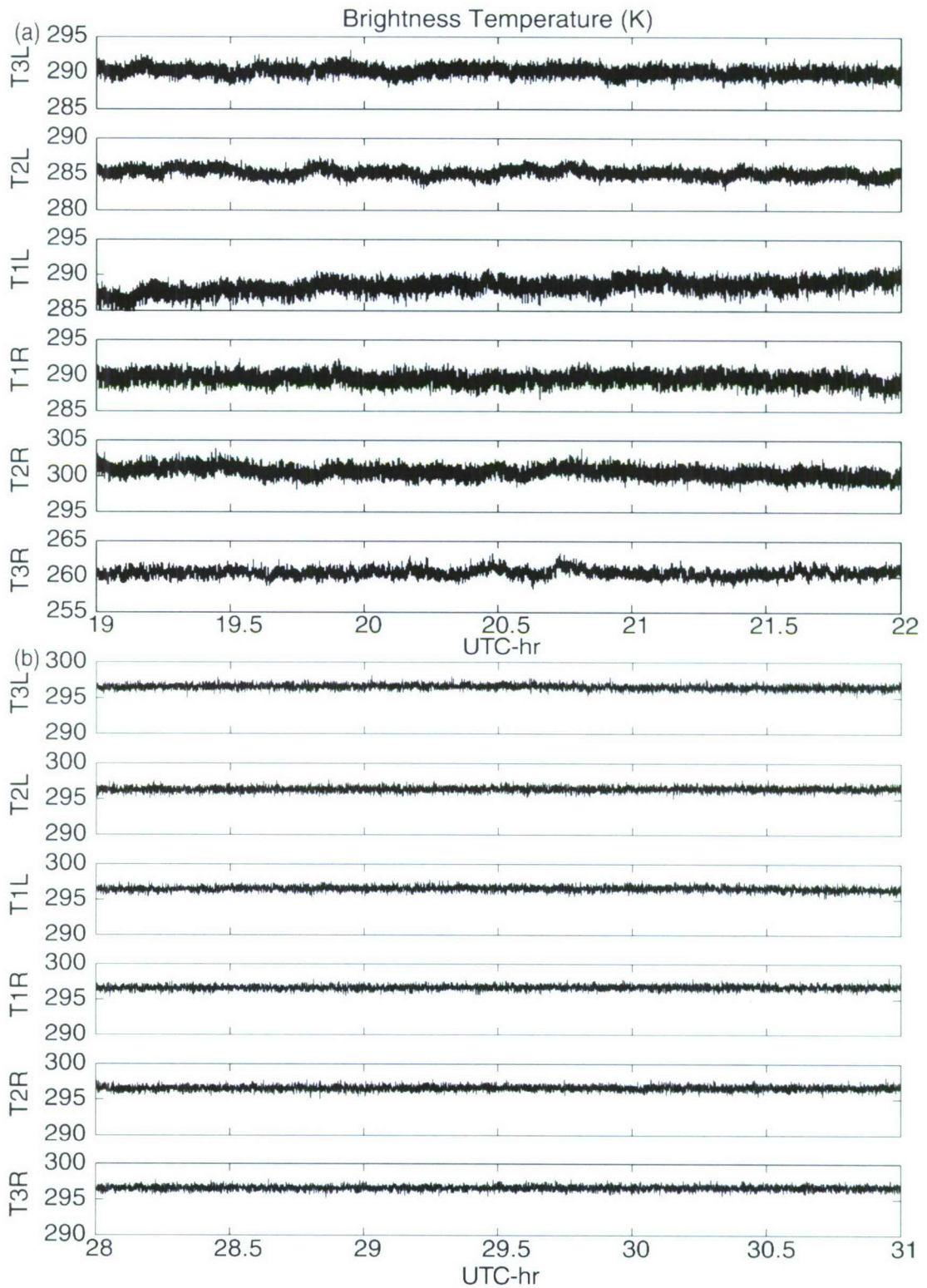

FIG. 2. Laboratory tests conducted over a 3-h period with STARRS isolated by microwave absorber showing brightness temperature sampled by all six beams as a function of time. (a) Preupgrade test of 1 May 2002 and (b) postupgrade test of 12 Nov 2003.

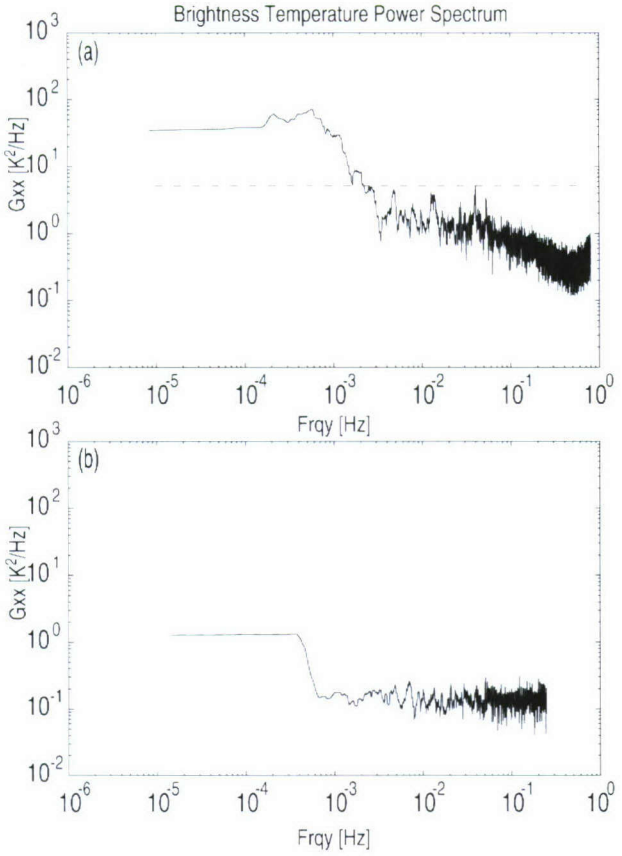

FIG. 3. Lomb-Scargle power spectrum of irregularly sampled beam 1-L data for 8.4-h laboratory tests conducted with STARRS isolated. (a) Preupgrade test of 14 Aug 2002 STARRS with 0.63-s mean sampling interval and (b) postupgrade 8.4-h laboratory test of 12 Nov 2003 with a 2.01-s mean interval.

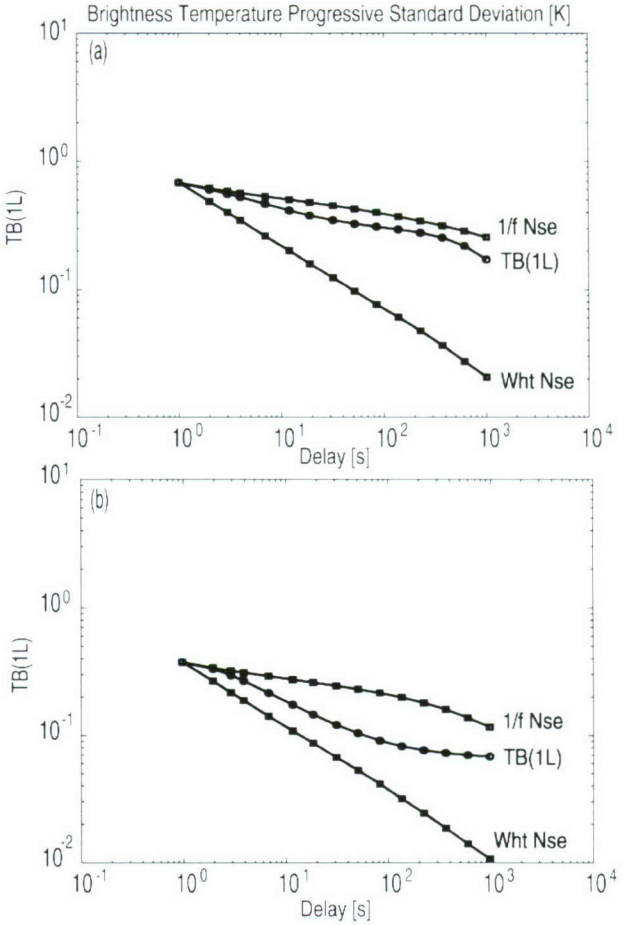

FIG. 4. Brightness temperature progressive std dev plots corresponding to the data presented in Fig. 3, after interpolation to a regular time base. (a) Preupgrade test of 14 Aug 2002 STARRS and (b) postupgrade 8.4-h laboratory test of 12 Nov 2003.

internal to the instrument. The possibility that the noise originated from fluctuations in the internal temperatures, not fully compensated for by the calibration procedure, was first investigated. It was discounted because the thermistor data showed that the internal temperatures increased gradually during the warm-up phase and remained steady thereafter. They exhibited no evidence of covariation with the observed brightness temperature fluctuations.

Power spectra obtained from the irregularly spaced data from an even longer laboratory test (8.4 h) collected on 14 August 2002 were computed using the Lomb–Scargle periodogram (Press et al. 1992). This handles irregularly sampled data and avoids the spectral distortions caused by interpolating at regular sample intervals for conventional analysis. The spectra indicate that the process was relatively broad banded, with T_b exhibiting a distinctly 'red " spectrum with an approximate $1/f$ spectral rolloff at higher frequencies (Fig. 3a). This is characteristic of a widely recognized and pervasive noise type-flicker noise, also known as 'brown " noise. It differs from white noise, which exhibits uniform power levels within the observed frequency band. While the variance of a stationary white noise process falls as $1/\sqrt{n}$ when filtered with a boxcar filter of length n samples, the variance of a $1/f$-noise process falls off much more slowly. Consequently, reliable estimates of brightness temperatures are only obtained (if at all) by long averaging times, which lead to an unacceptable reduction in temporal, and hence spatial, resolution. These effects are demonstrated by computing the 'progressive variance " function. [Wesson et al. (2003) first described this method in the caption to their Fig. 5, where it is referred to as a variant of the Allan deviation method.] This involves boxcar filtering a time series with progressively longer filters and calculating its variance, and its square root, the standard deviation, as a function of filter length (Fig. 4a). This performance measure may be contrasted with the 'clas-

sic" Allan deviation analysis, which computes the variance of differences between terms in a time series that are progressively farther apart—a method that tends to suppress short- to medium-term trends, which are presently our main concern (for more discussion of these performance measures, see Goodberlet 2003, unpublished manuscript; Goodberlet and Mead 2006). The adverse effects of the $1/f$-noise processes are particularly problematic in airborne data. The 6-min fluctuations appear as large-scale (~30 km) spatial variations in the observations for typical aircraft ground speeds of 90 m s^{-1}. They cannot be distinguished from environmental variability, unless salinity gradients are quite large.

Subsequent field deployments were confined to areas where strong salinity variations should be encountered. Surveys planned for the Adriatic Circulation Experiment (ACE; Fig. 5b) and for two regions in the northern Gulf of Mexico (Apalachicola Bay, Fig. 5a; Mississippi Sound, Fig. 6a; i.e., CoJet-V) were concentrated near the Po River, St. George Sound, and Mobile Bay, respectively, where the strong salinity gradients due to river and estuarine sources would likely dominate variability induced by instrument noise.

b. *Performance assessment in field*

Analysis of the data from the EuroSTARRS, ACE, and Apalachicola Bay/Mobile Bay surveys allowed STARRS to be effectively evaluated in the field, so that conservative performance criteria could be established. Apalachicola Bay (Fig. 5a) and Mobile Bay (Fig. 6a), with SSS contrasts of ~15 psu, provided the least demanding application, because relatively strong point sources dominated variations produced by the internal noise. The performance of STARRS for these locations was acceptable. ACE (Fig. 5b), with ~10 psu contrast, provided an intermediate case, in which short-term trends associated with the noise were quite evident, though the gross characteristics (location and intensity) of the Po River plume were quite well represented. EuroSTARRS (Fig. 5c) provided the most severe test, because the SSS gradients observed under the relatively homogeneous open ocean conditions that prevailed produced little salinity contrast (~1 psu), so that instrument noise dominated the weak ocean salinity signal.

We concluded from preliminary analysis of these first field deployments of STARRS that the instrument, though functional, exhibited limited performance in low-signal-to-noise environments. We further concluded that the original performance criteria (measures of NEDT and long-term calibration stability using repeated calibrations before and after each mission) were inadequate, to the extent that they did not allow for the

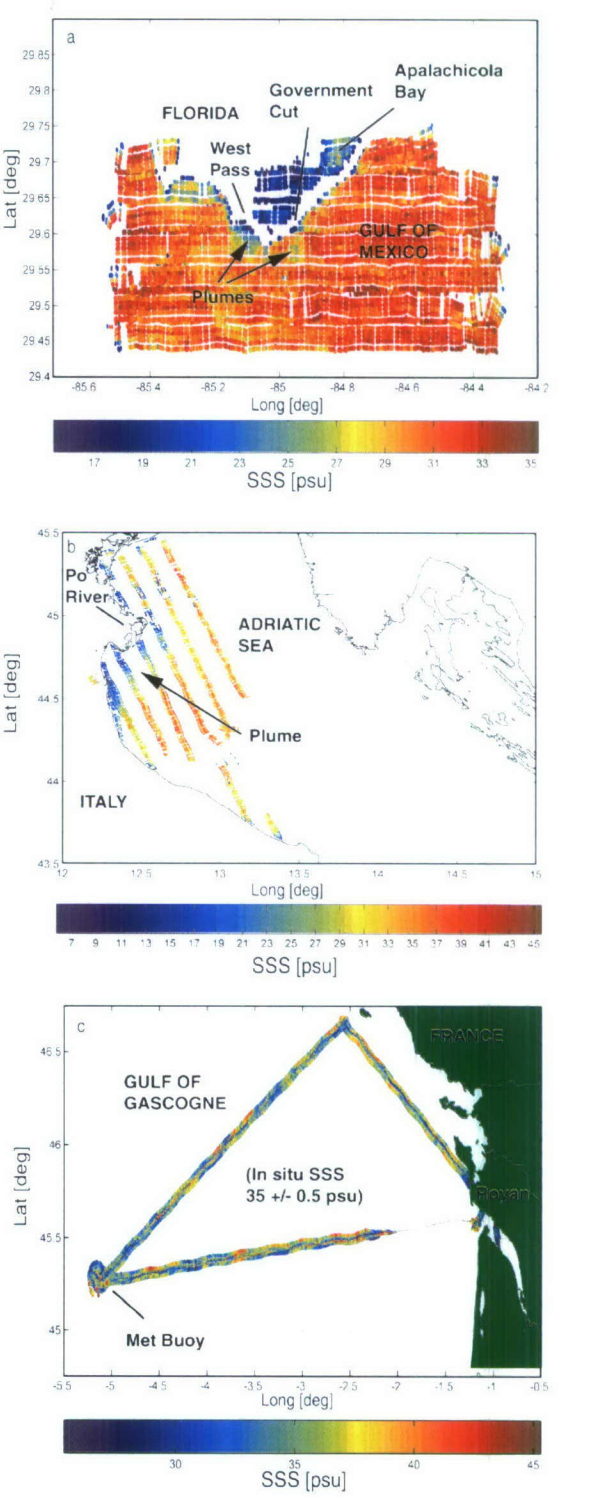

FIG. 5. STARRS preupgrade SSS maps obtained in various regions of high, medium, and low signal-to-noise ratio, respectively. (a) Apalachicola Bay on 2 Aug 2002 showing plumes of estuarine water emanating from passes during ebb tide, (b) northwestern Adriatic on 5 Oct 2002 showing Po River plume, and (c) Gulf of Gascogne in the Bay of Biscay on 17 Nov 2001 showing SSS measurements over a relatively homogenous region (35 ± 0.5 psu). The STARRS data, adjusted to match coincident in situ data (Etcheto et al. 2003) in the mean, show significant SSS variability (~± 5.0 psu) explained by internal instrument noise.

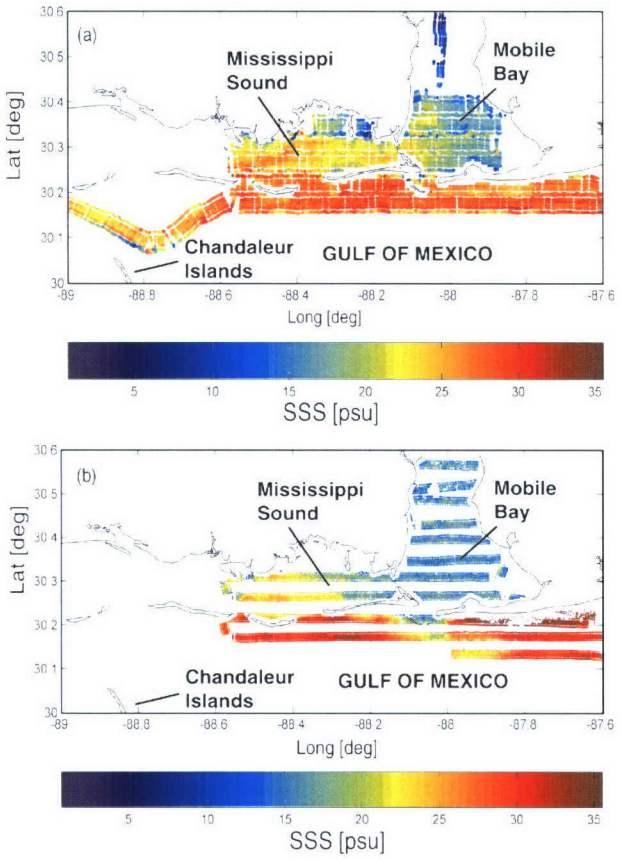

FIG. 6. STARRS SSS maps showing estuarine waters in Mobile Bay and Mississippi Sound and more saline water in the northern Gulf of Mexico. Mean beam salinities were adjusted to 25 psu in both maps to facilitate comparison. (a) Preupgrade map obtained on 12 Aug 2002 showing relatively noisy data and gaps due to calibration delays and (b) postupgrade map obtained on 8 Jun 2003 showing reduced noise levels and no calibration gaps.

possibility that $1/f$ noise would compromise the performance and calibration accuracy. In the future, these would be supplemented by measures such as progressive variance and Allan variation plots (Wesson et al. 2003; Goodberlet and Mead 2006), which better evaluate the instrument's short-term drift performance.

4. STARRS upgrade

a. Chopping rate

In the original STARRS design, the chopping process was implemented entirely in software, through computation of the radiometer output voltage ratio γ [defined in section 3a, Eq. (1)]. This provided considerable flexibility in setting the relative times spent observing the antenna and the two internal loads. The resulting slower chopping rate was offset by faster simultaneous sampling of each beam using six dedicated receivers. This contrasted with the SLFMR design in which chopping was implemented synchronously in hardware, but the beams were sampled sequentially, using a single receiver. The original STARRS sampling and chopping process was asynchronous, with a set of rules and parameters implemented in firmware.

The sampling scheme as implemented (Fig. 7a) consisted of two subcycles of interspersed antenna and warm and hot load observations. The antenna was sampled consecutively for periods of 13.8 s in 4 bursts totaling 55.2 s in each 85.8-s measurement cycle (64.3% of the cycle time in Table 2, column 4) at dwell times of 0.46 s (after analog filtering with a 1-s cut-off period). In contrast, the loads were sampled for only 1.4 s in 2 bursts totaling 7.2 s with dwells of 0.46 s in each measurement cycle. Chopping (i.e., computation of γ) was carried out every 0.46 s using successive antenna samples (when available) and linearly interpolated values of the warm and hot-plus-warm load temperatures T_h and T_w. The interpolants were obtained from the 1.4-s averaged samples acquired approximately twice per 85.8-s measurement cycle (because sampling was actually asynchronous, average timing values are shown). This was done to minimize overhead and maximize the time spent observing the antenna. It was justified by the assumed relative stability of the brightness

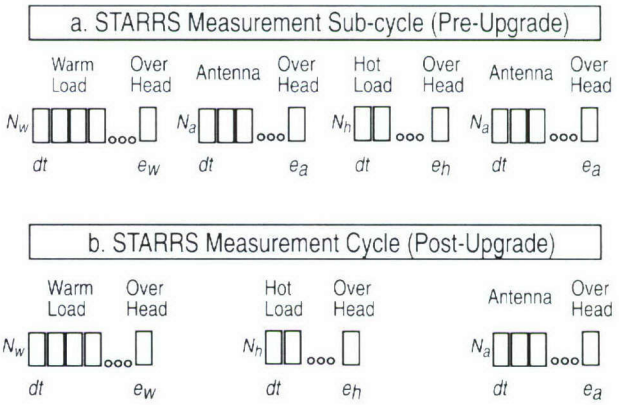

FIG. 7. STARRS sampling diagram for (a) preupgrade and (b) postupgrade versions of STARRS. The target antenna and loads are sampled at the fundamental sample interval dt. The number of such samples is N_w, N_h, and N_a for the warm load, hot load, and antenna targets, respectively. The corresponding overheads are e_w, e_h, and e_a, respectively. For each target i (= w, h, or a), the voltages associated with the N_i samples of length dt are averaged over a dwell time, $N_i\,dt$. Two measurement subcycles are required in the preupgrade version to allow the load voltages to be interpolated. The measurement cycle in this case is of duration 2 $[(N_w + 2N_a + N_h)\,dt + e_w + 2e_a + e_h]$. In the postupgrade case, it is $dt\,(N_w + N_h + N_a) + e_w + e_a + e_h$. Parameter values (see Table 2) are preupgrade: $N_w = N_h = 3$, $N_a = 30$, $dt = 0.46$ s, $e_w = e_h = 6.0$ s, and $e_a = 0.0$ s; and postupgrade: $N_w = 64$, $N_h = N_a = 32$, $dt = 0.0125$ s, $e_w = e_h = 0.1$ s, and $e_a = 0.16$ s.

temperatures of the reference loads, which are thermally controlled, compared with the signal from the antenna, which is subject to environmental variations. However, the large overhead (33.6%) associated with the reference noise samples produced "calibration" gaps in the antenna data, evident as sampling breaks in the preupgrade salinity maps (Figs. 5, 6a), and the chopping rate was effectively limited by the sampling speed of the AD converter and processing software. The load observations were interpolated to the times of the individual antenna samples to facilitate computation of γ at each 0.46-s sample interval.

Allowing user-specified parameters to determine the length of each measurement subcycle and how long particular components were sampled (e.g., antenna and warm or hot load) makes the process harder to analyze relative to conventional radiometers that chop at a constant rate with equal dwell times on the antenna and load (Goodberlet and Mead 2006). However, it allowed the time spent observing the antenna brightness temperatures to be deliberately increased relative to that spent observing the reference load brightness temperatures, with the intention of improving sensitivity.

The realization that STARRS suffered from significant internally generated $1/f$ noise prompted a detailed reexamination of the receiver design and AD conversion process. It also led us to adopt more comprehensive radiometer performance criteria. Increasing the chopping rate to remedy the $1/f$-noise performance required faster sampling and AD conversion and imposed proportionally higher overheads for switching antenna and load voltages. Furthermore, overall noise levels seemed to be higher than expected, given the manufacturer's specifications for key microwave components used in the receiver.

b. *Receiver and sampling performance*

Accordingly, ProSensing investigated the performance of each receiver and redesigned the I/O board to achieve faster sampling rates. A search of published literature and component manufacturer data sheets revealed that $1/f$ noise is characteristic of a wide variety of natural and man-made systems and, in particular, of certain electronic components utilized in the STARRS microwave receivers. Attention was focused specifically on the L-band RF amplifiers, which may be subject to variations in noise figure and gain variations, and particularly on the LNA, which is the critical first link in any analog receiver amplifier chain. The square law detector and video amplifier were also investigated, and it was found that $1/f$-noise generation is inherent in the silicon chip technology used in their construction. The specifications and internal functions of the third-order sigma-delta AD converter used in the I/O board were examined to see if its performance was adequate. More esoteric features, previously shown to influence SLFMR performance, were also considered. These included "box modes," which could be eliminated by separating and isolating key components, and "reentrant" filter responses, which could be avoided by careful choice of overlapping bandpass filter characteristics.

Against this background, a test bench was set up in ProSensing's laboratory to evaluate the response of a single STARRS receiver to a dummy load (effectively removing the antenna system as a possible source of the problem) and a new and faster I/O board was constructed to increase effective sampling rates and chopping frequency. Simultaneously with this effort, a SIMULINK (The Mathworks Inc.) simulation model of the test bench setup was created at NRL following methods developed by Burrage et al. (2002a) for the SLFMR. This was used to help investigate the response of the instrument to various component noise characteristics and to guide problem solving conceptually.

The results of these investigations are summarized as follows: the $1/f$ noise generated by the detector and video amplifier was assessed at well below the observed noise levels, and thus it was negligible. Bit errors occurring during AD conversion were a possible source of noise with a $1/f$ characteristic. Although the specifications of the sigma-delta converter used in STARRS indicated it was unlikely to account for the observed noise, it was upgraded to a faster flash-type AD converter to improve the sampling rate. The actual noise figures of the LNAs installed in the original STARRS receivers were found to fall short of the manufacturer's specifications; replacement with a new type reduced random receiver noise levels by a factor of 2, thus improving sensitivity. Most significantly, it was realized that trading off reference load observing time for longer antenna measurements within the measurement cycle significantly improved the NEDT, but ultimately compromised short-term instrument stability. While the assumption of reference noise brightness temperature stability over time scales of a few minutes is likely valid, it is not possible for the microwave receivers to measure these temperatures precisely at such time scales, because of the effects of amplifier noise and gain variations. Accurate cancellation of brightness temperature fluctuations because of such variations would thus not be possible, even if the interpolated reference load physical temperatures (measured by the temperature control system) were precise and γ was computed quite frequently (at 2.2 Hz in the original scheme, see Table 2). Relatively frequent chopping using actual,

rather than interpolated, reference load physical temperatures was required. On the test bench, faster chopping rates shifted the receiver noise behavior significantly closer to theoretical $1/\sqrt{n}$ performance; that is, flicker noise was significantly reduced. To achieve such rates in the complete multireceiver system, it was clear that a mix of hardware (under firmware control) and software would be needed in preference to the pure software approach adopted in the original design.

5. Upgrade performance assessment

Based on the engineering assessments, all six receivers and a spare were modified by replacing the LNAs with new components having improved noise figures (ProSensing Inc. 2003a). The Dicke switch was also replaced with a lower loss unit. Finally, the first bandpass prefilter, which is used to eliminate radio frequency interference, was moved from the antenna input to a point after the Dicke switch (Fig. 1b). The effect of this change was to eliminate out-of-band noise from the warm and hot load signal inputs, in addition to the antenna input. The new AD converter, which optionally implements chopper filtering in firmware, was also installed and the software was modified to accommodate new sampling modes and optionally faster chopping rates. The results of tests described next indicate that the system noise levels were significantly reduced.

a. Postupgrade laboratory tests

The performance of each of the newly modified receivers in the test bench setup was found to meet upgrade requirements, so a full system test was conducted. The upgraded instrument, with the newly modified receivers integrated with the L-band antenna, was tested in the laboratory by viewing a microwave absorber of constant brightness temperature (~292 K) and collecting data over a 100-min period (ProSensing Inc. 2003b, their section 5.0 and Fig. 5.1). The new digitizer was configured so that brightness temperature measurements were reported from each of the six receivers once every 1.0 s, and system thermal regulation was activated. Data analysis indicated that the desired single-measurement precision (NEDT) of 0.51 ± 0.02 K was achieved. Computation of the Allan deviations (plot not shown) revealed the extent to which the application of progressively longer averaging periods led to a reduction in data standard deviation. The Allan deviation fell below 0.1 K, when about 30 samples were averaged in succession. Furthermore, the Allan deviation fell to a minimum of 0.075 K after about 90 samples were averaged. In comparison, laboratory tests of the original STARRS sampling configuration yielded a 1-s NEDT of 0.4 ± 0.1 K that fell only to a minimum of 0.15 K after 30 samples were averaged. Thus, the new configuration when compared with the original exhibited a significant reduction in thermal noise, with only modest data averaging.

TABLE 3. Std dev of STARRS calibrated T_b for a microwave-absorber target at ambient temperature for beams 1–6 [3L, 2L, 1L, 1R, 2R, and 3R]. (a) Preupgrade and (b) postupgrade.

a. Std dev (K) for preupgrade test 01 May 2002

Beam	Mean	1-s std dev	12-s std dev	24-s std dev
1	290.16	0.48	0.34	0.31
2	285.15	0.47	0.37	0.35
3	288.36	0.63	0.47	0.41
4	289.55	0.59	0.42	0.37
5	300.52	0.53	0.38	0.35
6	260.49	0.48	0.39	0.37
	N	1	12	24
	Mean:	0.53	0.39	0.36
	1-s std dev $\sqrt{N}$	0.53	0.15	0.11

b. Std dev (K) for postupgrade test 12 Nov 2003

Beam	Mean	1-s std dev	12-s std dev	24-s std dev
1	296.61	0.55	0.3	0.24
2	296.37	0.54	0.28	0.21
3	296.56	0.51	0.3	0.23
4	296.69	0.5	0.27	0.2
5	296.62	0.54	0.27	0.21
6	296.64	0.5	0.27	0.2
	N	1	12	24
	Mean:	0.52	0.28	0.21
	1-s std dev $\sqrt{N}$	0.52	0.15	0.11

To obtain more precise estimates of NEDT, we selected longer records (3 h or more), and after removing a linear trend, we estimated their simple standard deviation (Table 3). We did this for data interpolated and resampled to 1-s intervals (column 3) and also for the same data averaged over and resampled on 12- and 24-s time scales (columns 4, 5). The results of this analysis show that the pre- and postupgrade 1-s NEDTs defined in this way are virtually indistinguishable, while the postupgrade 12- and 24-s standard deviations are significantly smaller, though not so small as would be predicted for a theoretical white noise process.

Thus, while the 1-s NEDT was similar after the upgrade, the longer-term performance or stability over periods of ~10 s to several minutes or more was substantially improved. The relative constancy of the mean brightness temperatures for each beam in the postupgrade case also shows that the precision of the instrument calibration improved significantly.

A dramatic improvement in performance is seen by comparing the time series obtained from the preup-

grade 3-h test of 1 May 2001 (Fig. 2a), which shows the quasi-periodic 6-min variability, with the postupgrade laboratory test of 12 November 2003, which lacks this feature (Fig. 2b). The Lomb-Scargle power spectrum of the uninterpolated data obtained 14 August 2002 (Fig. 3a) shows a characteristic red spectrum with a tendency of $1/f$ rolloff at frequencies above 4×10^{-3} Hz (corresponding to periods less than 250 s). In contrast, the spectrum from the 12 November 2003 test (Fig. 3b) shows noise levels that are as much as 2 orders of magnitude lower at lower frequencies, dropping to a white noise "floor" at frequencies above 5×10^{-4} Hz (periods less than 2000 s, 33.3 min). The corresponding progressive standard deviation plots in Figs. 4a,b show that the preupgrade deviations closely follow the theoretical $1/f$ pattern, while the postupgrade deviations more closely approximate the theoretical white noise pattern. These results demonstrate that the upgrade has significantly improved the instrument performance over time scales extending from a few seconds to about half an hour, so that target T_b variations on even longer time scales can be more faithfully reproduced.

b. *Optimizing sampling times*

In the original preupgrade version of STARRS, antenna sampling was interspersed with the warm and hot load sampling, and the antenna samples were relatively long. The averaged warm and hot load voltages were linearly interpolated to the times of each fundamental antenna sample, using data from two successive subcycles to compute γ (see Table 2). In the postupgrade version, the warm and hot load average voltages are used to compute γ directly at the end of each measurement cycle, without load voltage interpolation. The targets are sampled rapidly at 0.0125-s intervals, and the voltages are boxcar averaged to produce effective dwell times of 0.4 s for the antenna and warm load and 0.8 s for the hot load (Table 2; Fig. 7b). In the current implementation, chopping (γ calculation) is performed in software at 1.96-s intervals, without any interpolation. The AD converter can be programmed to perform chopping digitally in hardware, at a faster rate, but a significantly greater fraction of the sampling time is then lost to load-switching overheads.

More recent investigations (Goodberlet and Mead 2006) show there are significant uncertainties in measuring both the antenna and load brightness temperatures and that the optimal combination of antenna and load dwell times for a two-load radiometer, such as STARRS, depends on the target temperature, or more precisely, its temperature relative to the load temperatures. In the upgrade case, the dwell times and chopping period presented in Table 2 were optimized with respect to NEDT using the procedure described by Goodberlet and Mead (2006).

c. *Postupgrade field tests*

Field tests of STARRS, following the upgrade, were conducted in Mississippi Bight and over Mobile Bay and its entrance into the Mississippi Sound in the northern Gulf of Mexico during 5–8 June 2003. Test flights over Mississippi Bight were conducted east of the Chandeleur Islands (see Fig. 6 for location) in a region of relatively homogeneous SST and SSS conditions (Fig. 8a). The flights were centered over NOAA weather buoy NDBC 42007, which provided in situ surface temperature, wind, and wave data. Three flights were conducted in the vicinity of the buoy on 6 and 7 June 2003 under partly cloudy conditions, with a number of transects at various altitudes and orientations (generally, east–west, north–south, and either northeast or southwest). Some (outbound) transects were closely repeated by flying along an approximately parallel track but in a reversed (inbound) direction.

Pairs of outbound and inbound transects were approximately parallel (Fig. 8a). To facilitate comparisons between them, the data from both transects were projected orthogonally onto a bisecting line lying equidistant between and approximately parallel to these transects. In a representative series of data from the east–west transect pair obtained on 6 June 2003 (Fig. 8b), it is evident that the larger features of a 5-km or longer scale observed on the outbound transect were faithfully reproduced along the inbound transect, while smaller-scale features on the order of 1 km were apparently dominated by residual noise, because the outbound and inbound values were uncorrelated. Differences on intermediate spatial scales might be explained by instrument drift, but could also be caused by actual changes in sea surface conditions, such as advective displacements of a spatially varying SST and SSS pattern (e.g., due to wind or tide), and possibly changes in sea state, related to wind gusts.

Statistics of the differences between the projected outbound and inbound transect values (mean and standard deviation) were also computed for each bisector. The difference statistics (Table 4) reveal the extent to which the inbound and outbound transects differ from one another. Mean differences in microwave brightness temperatures ranged in magnitude from 0.0 to 0.9 K with an overall mean of 0.4 K, while standard deviations, which are higher in the outboard beams because of aircraft roll variations, ranged from 1.1 to 2.1 K with a global value of 1.7 K. The along-track mean salinity differences for the six beams, which have been corrected for roll variations, ranged in magnitude from 0.0

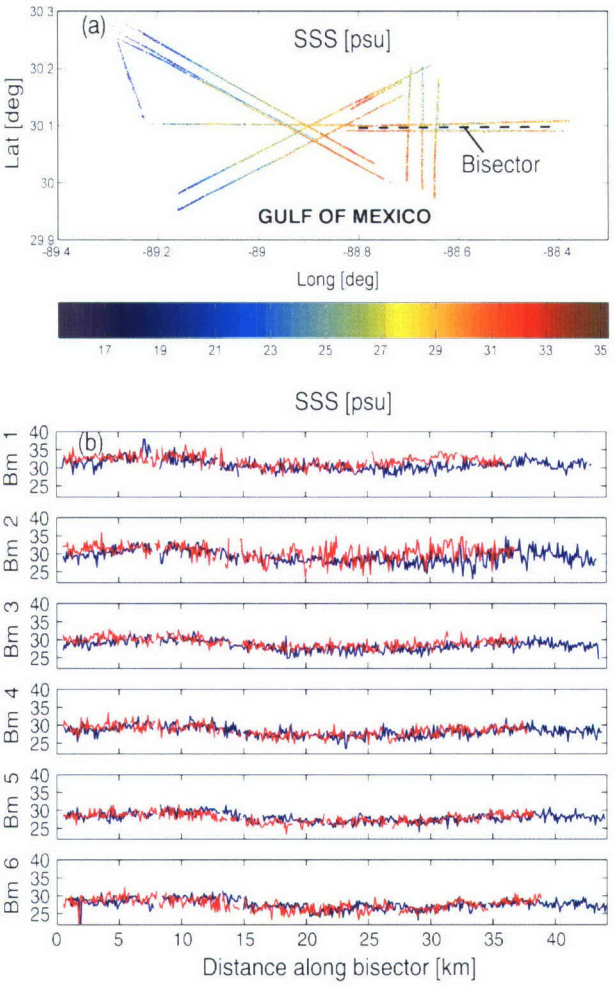

FIG. 8. (a) One of three postupgrade SSS maps obtained in a star-shaped flight pattern over Mississippi Bight during 6–7 Jun 2003. Some tracks were closely repeated by flying parallel in the reverse direction. (b) Spatial series of data appearing in the eastern east-west segment in (a). The data were projected onto the bisecting line, plotted as a function of distance along that line, and analyzed statistically (see Table 4). Outbound tracks (blue) and inbound tracks (red) show good agreement on scales on the order of 5 km or longer, while fluctuations on scales on the order of 1 km are mostly uncorrelated.

TABLE 4. Difference statistics of T_b and SSS for STARRS flight over Mississippi Bight on 6 Jun 2003 from nearly parallel east–west transects.

Beam number	Mean T_b (K)	Mean SSS (psu) (K)	Std dev T_b (K)	Std dev SSS (psu)
1	0.75	−1.16	2.06	1.95
2	0.85	−1.36	2.03	2.59
3	0.56	−0.82	1.1	1.55
4	0.17	−0.24	1.21	1.67
5	−0.01	0.11	1.83	1.47
6	0.05	0.03	1.97	1.91
Overall	0.4	−0.57	1.7	1.9

to 1.4 psu with a global mean (combining all beams) of 0.6 psu, and the standard deviations ranged from 1.5 to 2.6 psu with a global value of 1.9 psu. Because the infrared radiometer is nadir viewing, beam-to-beam SST differences are not meaningful, so they are not shown. The global mean SST difference of 0.015°C and global standard deviation of 0.2°C indicate only minor contributions to the salinity differences, through their effects on the emissivity model function (Klein and Swift 1977) and hence on brightness temperature values, T_b. The differences may be caused by actual salinity changes (e.g., due to tidal advection), changes in surface roughness due to wind and errors in measured or modeled environmental influences on emissivity (other than SST and SSS) such as incidence angle, or by instrument noise. In any case, the statistics indicate the degree to which noise might dominate the signal at time (and length) scales that were problematic prior to the upgrade. They also give an indication of the reliability of the measurements over intermediate observational time scales (~minutes) and an estimate of the combined environmental and instrumental error (sampling error) experienced in the field.

1) FIELD NEDT

We can use field data obtained over relatively homogeneous regions to compute an approximate value for NEDT, while recognizing that environmental variability and errors in environmental corrections will tend to inflate the value above what would be obtained under controlled conditions in the laboratory. Consequently, a field-derived NEDT will yield a useful upper bound to estimates that would be obtained in laboratory calibrations, which do not account for interfering factors such as aircraft influence on sampling noise and antenna pattern.

Taking the first spatial difference in the along-track direction of the (across track) differences between the inbound and outbound transects eliminates temporal and spatial trends and gives an indication of the short-term noise levels, and thus of the effective NEDT, as realized in the field. If this is done for 6 June 2003, then data values on the order of 1.5 K are obtained. However, these values are essentially raw brightness temperatures, without any correction for aircraft attitude and environmental influences. A better estimate can be obtained by computing what we term the nadir equivalent brightness temperature, as follows: raw T_b values are used together with SST to compute SSS using the emissivity model function (Klein and Swift 1977) and to apply corrections for aircraft roll and environmental

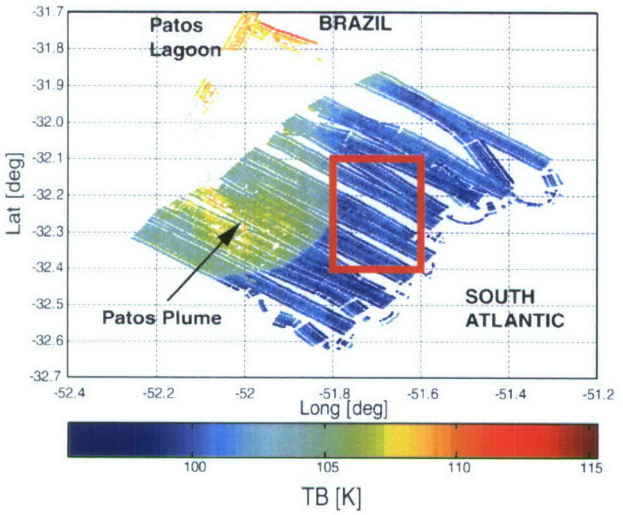

FIG. 9. Postupgrade STARRS survey of estuarine plume from Patos Lagoon obtained on 1 Sep 2003. Equivalent nadir-view T_b (K) is computed using environmentally and roll-corrected SSS and SST. Unmodeled environmental effects and instrument noise remain. The std dev of 0.7 K (equivalent 1-s NEDT 0.9 K) obtained from data falling inside the red box places an upper bound on instrument sensitivity in the field.

influences such as atmospheric O_2 absorption. The emissivity model is then used to invert the SSS and SST values to equivalent T_b values for a zero-incidence angle (nadir) view. The resulting T_b values are thus corrected for beam geometry and known environmental influences, but variability remains because of unmodeled environmental influences and instrument noise. Nadir-view T_b values in the relatively homogenous area enclosed by the frame for the Patos Lagoon outflow plume survey (Fig. 9) yield an overall T_b standard deviation of 0.7 K for a 1.8-s median sample interval. The corresponding 1-s NEDT is 0.9 K. This is larger than but close to NEDT values computed in the laboratory, showing that a near upper bound to NEDT can be obtained from field data gathered in relatively homogenous regions, if nadir equivalent brightness temperatures are first computed. This is a useful performance measure because it is obtained under operational conditions that cannot be reproduced in the laboratory. Because it includes the effects of unmodeled environmental corrections, it is also a useful indicator of overall system performance.

2) CALIBRATION DRIFT

The field data can also be used to assess the magnitude of calibration drift or stability. Data from the 8 June 2003 flight were processed using regression coefficients from laboratory calibrations on 30 May 2003, within 1 week of the experiment, and on 20 November 2003, about 6 months later, and the resulting calibrated brightness temperatures were compared. The change in mean T_b for each of the six beams ranged from −2.26 to 1.24 K, and the overall mean changed by −0.85 K, a drop of less than 1 K over a 6-month period. If linear, this suggests a calibration drift of about 0.38 K month^{-1} per beam, and about 0.14 K month^{-1} overall, a month being a typical time delay between field deployment and laboratory calibration, accounting for overseas shipping and installation delays. This may be compared with the beam-averaged calibration drift of 1.6 K month^{-1} estimated for the preupgrade period spanning EuroSTARRS.

As a final qualitative field test of the instrument, STARRS was flown in a mapping flight over Mobile Bay (Fig. 6b). This flight followed a set of transects similar to that used during the CoJet-V flights conducted on 12 August 2002, prior to the upgrade (Fig. 6a). After adjusting the mean salinities on each beam to 25 psu to eliminate bias errors, comparison of the two maps reveals that noise levels have been significantly reduced, both on short and medium time scales. In the later flight, there are no calibration gaps, there is little evidence of along-track variations in salinity due to noise, and beam-to-beam biases estimated prior to the mean adjustment are small. The majority of the variation is spatially coherent and appears to be associated with large-scale salinity variations, which suggests that the variations are real.

6. Discussion

The completed STARRS L-band radiometer upgrade involved enhancements to both the individual microwave receivers and the AD conversion hardware and firmware. Laboratory tests revealed a significant improvement in instrument noise performance on time scales of 2–100 s, while stability over the problematic intermediate time scales of several minutes was dramatically improved. The improvement in stability was obtained, according to at least one estimate, at the cost of a marginal deterioration of the 1-s NEDT performance. Field tests also demonstrated significant improvements in performance with respect to sensitivity, or NEDT, measured on 2–10-s time scales, and noise spectrum, with close to $1/\sqrt{n}$ variance scaling over a time scale of a few seconds to tens of minutes.

The reduction in short-term noise fluctuations was achieved by replacing the low- noise amplifiers in the receivers and by replacing or relocating other critical front-end components. This, coupled with enhancements to the AD conversion processes and chopping

procedures, resulted in a significant "whitening" of the noise spectrum and made medium time-scale averaging significantly more effective in removing noise. It largely eliminated incoherent short-term drift in the observed brightness temperatures measured by each of the beams. Optimization of the dwell time used for sampling the antenna and reference load signals further enhanced performance.

All these improvements were achieved without changing the thermal regulation of the instrument, demonstrating that the performance of that subsystem was neither a factor in the appearance of the spurious fluctuations nor in their remediation. While good thermal regulation is desirable in most radiometer systems and applications, careful calibration using the internal temperatures of the system as independent variables in determining the calibration coefficients can effectively compensate for fluctuations in these variables. Presently, internal temperatures are sampled at 30-s intervals and resolved digitally to 0.05°C. Calculations based on the calibration coefficients indicate that internal temperature measurement errors of 0.1°C could produce comparable brightness temperature errors of 0.1 K. Thus at its current sensitivity level of 0.52 K (NEDT), STARRS performance could benefit from improved resolution of the internal temperatures. Drift in the calibration of the internal temperature sensors, which once installed are difficult to calibrate individually, could contribute to long-term instrument calibration drift. Drift due to such factors as thermistor aging and vibration can best be mitigated by routine calibration of the entire radiometer. Nevertheless, improvements are possible: the calibration method, which involves allowing the instrument to warm and cool while observing each target, is problematic because internal temperatures tend to covary. This can make reliable regression coefficient determination difficult; the temperatures are not truly independent, so the regression matrix tends to be ill conditioned. Methods to differentially heat and cool individual components during calibration could be employed to produce a wider spread of variable values to alleviate this problem. It is also difficult to avoid internal temperature gradients during operation, considering the differing thermal characteristics of the various components and the proximity of the cold airstream passing the radome. Precise internal temperature calibration and equilibration is thus not possible. Methods to actively circulate air within the instrument enclosure could be considered to reduce these gradients. However, care would be needed to avoid temperature fluctuations due to turbulence and electrical interference or external heating caused by the circulation system.

Leaving aside possible future enhancements to the thermal regulation system, long-term stability and calibration drift have improved as a result of the hardware upgrade, as evidenced by reductions in calibration regression residuals and more constant calibration gain and offset coefficients. This could be partly due to improved statistical reliability in the calibration procedures resulting from the enhanced noise performance. In any case, improved noise performance has resulted in more consistent calibrations of STARRS, with estimated beam calibration drifts of better than 0.4 K month^{-1}. Despite this improvement, pre- and postcalibration for missions of several days' duration are still considered desirable to monitor possible calibration changes.

7. Conclusions

Prior to the recent hardware and software upgrades, successful applications of STARRS were confined to coastal survey regions exhibiting strong salinity gradients, such as those found in the tidally dominated plumes emanating from Apalachicola Bay and from Mobile Bay in the vicinity of its entrance into Mississippi Sound and Mississippi Bight. Application to mapping of the Po River outflow in the northern Adriatic was also successful, though marginally so in certain areas. Moderately high levels of medium-term drift ($1/f$ noise) were experienced in all the receivers. The successful upgrade expanded the range of applications of STARRS to oceanographic situations commonly encountered on the outer continental shelf. Here, circulation is influenced by large-scale estuarine inputs, upwelling driven by along-shelf wind fluctuations or mesoscale eddies for which typical salinity gradients are significantly lower.

STARRS was recently deployed in such a setting as a component of the Plata project (Pérez et al. 2006). The upgraded instrument was mounted on a Uruguayan Air Force Casa 212 aircraft and successfully used to map the La Plata River plume during August–September 2003, within a zone extending from Mar del Plata, Argentina, to Florianopolis, Brazil, from the coast to beyond the 200-m isobath. Analysis of the data shows generally low noise levels, with no indication of medium-term drift associated with $1/f$ noise. Furthermore, when STARRS was recalibrated in mid-November, after the Plata experiment, the calibration had changed little from that obtained in late May, immediately after the upgrade. This confirms that the long-term stability of the instrument has also been improved, or at least is more readily apparent, because of the lower noise levels and more reliable calibration.

The improvements in STARRS sensitivity on time scales longer than 1 s allow other sources of error in salinity retrievals, which have previously been below the noise level, to be addressed. At the level of sensitivity now achievable with STARRS, sea surface roughness effects on L-band emissivity, which were detected before the upgrade during EuroSTARRS (Gabarró et al. 2003; Etcheto et al. 2004), can be more precisely determined for future applications.

The STARRS C-band radiometer was designed to measure this roughness influence. It is a multichannel instrument that samples sea surface brightness temperature at six programmable frequencies polled by a single receiver (in the manner of the SLFMR) through a single nadir-viewing beam. The C-band design involved a relatively high degree of isolation among the various components (as in the upgraded L-band radiometer), but it used a similar sampling scheme to the original L-band system, so it also suffered $1/f$ noise resulting in response fluctuations with time scales of a few minutes. The instrument was recently upgraded using similar methods to those used here for the L-band radiometer, and the fluctuations were successfully eliminated.

Improvements in the performance of both the L- and C-band instruments will facilitate detecting salinity signals in cool temperate and subpolar regions, where better sensitivity in measuring both T_b and SST is needed. However, the resulting lower T_b signal-to-noise ratio could be partly offset by fresher water found in such regions, for example, due to snowmelt and associated freshwater runoff. As cloud cover is particularly problematic in both the tropical and polar regions, alternative methods of measuring SST that are not hindered by cloud will also need to be developed. The upgraded STARRS six-channel C-band radiometer offers the potential to provide simultaneous retrieval of both SST and surface roughness data needed for L-band salinity retrieval. Because C-band microwave radiation penetrates atmospheric water vapor, clouds, and even light rain, the C-band radiometer could facilitate an "all-weather" capability for airborne salinity mapping, at least under conditions normally tolerated by light aircraft.

With the recent performance improvements, STARRS can be used to address a wide variety of technical issues to further refine sea surface temperature, roughness, and salinity retrieval algorithms. It will also be useful for observing mesoscale circulation on outer continental shelves and for detecting relatively subtle salinity gradients associated with far-field dispersal and merging of large-scale plumes spanning the continental shelf and slope. Its potential for application as a "test bed" for the development and validation of satellite SSS missions already exploited during the EuroSTARRS mission and prior to the current hardware upgrade can also be expanded in the period leading up to and immediately following the launch of the SMOS and Aquarius missions currently being planned by ESA and NASA, respectively.

Acknowledgments. The STARRS development work was supported by the Office of Naval Research as part of the NRL's basic research project Salinity-Driven Advection in Littoral Deep Areas (SALIDA) under Program Element 0602435N and by ONR Global through Navy International Cooperative Program in Science and Technology (NICOP) Grant N00014-02-1-0295 led by Edmo Campos, University of Sao Paulo. D. Burrage also acknowledges early administrative support from the Department of Marine Science of the University of Southern Mississippi. The expert assistance of the captains and crews of the Piper Navajo aircraft, owned and operated by Rick Aviation, Inc., and of the Dornier 228 aircraft, owned and operated by the German Aerospace Agency (DLR), is gratefully acknowledged. Funding support for the EuroSTARRS project came from the European Space Agency. European EuroSTARRS participants are thanked for helping to identify and diagnose radiometer performance issues. NOAA provided J. Miller with access to the original SLFMR, and previous work by D. Burrage on the Australian SLFMR was supported by the Australian Research Council and the Australian Institute of Marine Science.

REFERENCES

Burrage, D. M., M. A. Goodberlet, and M. L. Heron, 2002a: Simulating passive microwave radiometer designs using SIMULINK. *Simulation,* **78,** 36–55.

——, M. L. Heron, J. M. Hacker, T. C. Stieglitz, C. R. Steinberg, and A. Prytz, 2002b: Evolution and dynamics of tropical river plumes in the Great Barrier Reef: An integrated remote sensing and in situ study. *J. Geophys. Res.,* **107,** 8016, doi:10.1029/2001JC001024.

——, J. Miller, D. Johnson, J. Wesson, and J. Johnson, 2002c: Observing sea surface salinity in coastal domains using an airborne surface salinity mapper. *Proc. IEEE/MTS Oceans 2002,* Vol. 4, Biloxi, MS, IEEE, 2014–2024.

——, M. L. Heron, J. M. Hacker, J. L. Miller, T. C. Stieglitz, C. R. Steinberg, and A. Prytz, 2003: Structure and influence of tropical river plumes in the Great Barrier Reef: Application and performance of an airborne sea surface salinity mapping system. *Remote Sens. Environ.,* **85,** 204–220.

Dicke, R. H., 1946: The measurement of thermal radiation at microwave frequencies. *Rev. Sci. Instrum.,* **17,** 268–274.

D'Sa, E. J., J. B. Zaitzeff, C. S. Yentsch, J. L. Miller, and R. Ives, 2001: Rapid remote assessments of salinity and ocean color in Florida Bay. *The Everglades, Florida Bay, and Coral Reefs of*

the Florida Keys: An Ecosystem Sourcebook, J. W. Porter and K. G. Porter, Eds., CRC Press, 451–459.

Etcheto, J., S. Contardo, S. Morvan, A. Lourenco, and J. Boutin, 2003: Oceanographic conditions during EuroSTARRS flights over Atlantic and Mediterranean Transit. *Proc. First Results Workshop on EuroSTARRS, WISE, LOSAC Campaigns*, Toulouse, France, European Space Agency, 61–65.

—, and Coauthors, 2004: Wind speed effect on L-band brightness temperature inferred from EuroSTARRS and WISE 2001 field experiments. *IEEE Trans. Geosci. Remote Sens.*, **42,** 2206–2213.

GabarróC., J. Font, A. Camps, and M. Vall-Llossera, 2003: Retrieved sea surface salinity and wind speed from L-band measurements for WISE and EuroSTARRS campaigns. *Proc. First Results Workshop on EuroSTARRS, WISE, LOSAC Campaigns*, Toulouse, France, European Space Agency, 163–171.

Goodberlet, M. A., and C. T. Swift, 1993: A remote sensing system for measuring estuarine and coastal ocean surface salinity. Progress Rep. 2, NOAA Contract 50-DKNA-1-00119, Quadrant Engineering, 111 pp.

—, and J. B. Mead, 2006: Two-load radiometer precision and accuracy. *IEEE Trans. Geosci. Remote Sens.*, **44,** 58–67.

—, C. T. Swift, K. P. Kiley, J. L. Miller, and J. B. Zaitzeff, 1997: Microwave remote sensing of coastal zone salinity. *J. Coastal Res.*, **13,** 363–372.

Hach, J.-P., 1968: A very sensitive airborne microwave radiometer using two reference temperatures. *IEEE Trans. Microwave Theory Tech.*, **16,** 629–636.

Kerr, Y. H., P. Waldteufel, J.-P. Wigneron, J. Martinuzzi, J. Font, and M. Berger, 2001: Soil moisture retrieval from space: The Soil Moisture and Ocean Salinity (SMOS) mission. *IEEE Trans. Geosci. Remote Sens.*, **39,** 1729–1735.

Klein, L. A., and C. T. Swift, 1977: An improved model for the dielectric constant of sea water at microwave frequencies. *IEEE Trans. Antennas Propag.*, **25,** 104–111.

Lagerloef, G. S. E., C. T. Swift, and D. M. Le Vine, 1995: Sea surface salinity: The next remote sensing challenge. *Oceanography*, **8,** 44–50.

Le Vine, D. M., A. Griffis, C. T. Swift, and T. J. Jackson, 1994: ESTAR: A synthetic aperture microwave radiometer for remote sensing applications. *Proc. IEEE*, **82,** 1787–1798.

—, G. S. E. Lagerloef, S. Yueh, F. Pellerano, E. Dinnat, and F. Wentz, 2006: Aquarius mission technical overview. *Proc. IGARRS 2006*, Denver, CO, IEEE, 1678–1680.

Miller, J. L., 2000: Airborne remote sensing of salinity. *Backscatter: Newsletter of the Atlantic Centre for Remote Sensing of the Oceans*, Atlantic Centre for Remote Sensing of the Oceans, 24–27.

—, and M. A. Goodberlet, 2004: Development and application of STARRS–A next generation airborne salinity imager. *Int. J. Remote Sens.*, **25,** 1319–1324.

——, and J. B. Zaitzeff, 1998: Airborne salinity mapper makes debut in coastal zone. *Eos, Trans. Amer. Geophys. Union*, **79,** 173–177.

Péez, T., J. Wesson, and D. Burrage, 2006: Airborne remote sensing of the Plata plume using STARSS. *Sea Technol.*, **47,** 31–34.

Press, W. H., B. P. Flannery, S. A. Teukolsky, and W. T. Vetterling, 1992: *Numerical Recipes in C*. 2nd ed. Cambridge University Press, 994 pp.

ProSensing Inc., 2001: Salinity Temperature and Roughness Remote Sensor (STARRS). Final Rep. Naval Research Laboratory–SSC Contract N00173-00-C-6014, ProSensing Inc., 34 pp.

—, 2002: STARRS Radiometer Informal Report, July 29. Naval Research Laboratory–SSC Contract N00173-03-P-69908 Rep., ProSensing Inc., 6 pp.

—, 2003a: STARRS radiometer upgrade—Progress Report, May 21. Naval Research Laboratory–SSC Contract N00173-03-P-6908 Rep., ProSensing Inc., 5 pp.

—, 2003b: STARRS radiometer upgrade test data–Final Report, June 4. Naval Research Laboratory–SSC Contract N00173-03-P-6908 Rep., ProSensing Inc., 8 pp.

Prytz, A., M. L. Heron, D. Burrage, and M. Goodberlet, 2002: Calibration of the scanning low frequency microwave radiometer. *Proc. IEEE/MTS Oceans 2002*, Vol. 4, Biloxi, MS, IEEE, 2003–2007.

Skou, N., 1989: *Microwave Radiometer Systems*. Artech House, 162 pp.

Ulaby, F. T., R. K. Moore, and A. K. Fung, 1981: *Microwave Remote Sensing Active and Passive*. Vol. 1. Addison-Wesley, 456 pp.

Wesson, J., D. Burrage, and J. Miller, 2003: STARRS calibration and noise issues for EuroSTARRS. *Proc. First Results Workshop on EuroSTARRS, WISE, LOSAC Campaigns*, Toulouse, France, European Space Agency, 67–72.